Lab on a Chip

PAPER

View Article Online
View Journal | View Issue

Cite this: *Lab Chip*, 2026, **26**, 830

Formation of an endometrial epithelial monolayer in a microfluidic device with human tissue-derived endometrial organoids

Seung-cheol Shin,†[a] Yale Hahm,†[a] Yeju Jeong,[b] Yup Kim,[f] Junsik Park,[g] Ji Hun Yang,[hi] Jin-A Kim,[b] Jihee Won,*[e] Seok Chung*[abc] and Jung-Yun Lee*[d]

Received 18th March 2025,
Accepted 15th December 2025

DOI: 10.1039/d5lc00278h

rsc.li/loc

The endometrium is the uterine lining that supports implantation and pregnancy. Existing *in vitro* systems only partly capture epithelial structure and function. We built a microfluidic model of the human endometrial epithelium using patient-derived organoids and defined a parameterized device and ECM conditions that yield a stable, polarized monolayer on chip. We specify the geometry, surface treatments, and collagen-based hydrogel or coating conditions, and we link these parameters to epithelial morphology and barrier integrity readouts. The epithelial layer maintains histologic features and endometrium-relevant markers and shows hormone-responsive transcript profiles. We quantify donor-to-donor variability across two donors and use it as a design constraint for reproducible culture. Because stromal and immune components shape the reproductive microenvironment, we will extend this platform to modular multicellular co-cultures that incorporate these elements.

Introduction

The endometrium—the inner lining of the uterus—drives mammalian reproduction. It has two layers, the functionalis and the basalis, each with glandular epithelium and stroma. The functionalis expands under estradiol (E2), then differentiates under progesterone (P4) into ciliated and secretory phenotypes; progesterone withdrawal triggers breakdown and shedding during menstruation. The basalis abuts the myometrium, persists through the cycle, and regenerates the functionalis.[1–4] Estrogen and progesterone receptors (ERs and PRs) show phase- and cell type-specific expression: the ER predominates in the proliferative phase, and the PR becomes active in the secretory phase.[5] Glandular cells produce progestogen-associated endometrial protein (PAEP, glycodelin), which rises in the secretory phase under P4 regulation.[6] Disrupted remodeling links to infertility, endometriosis, and pregnancy complications.[7]

Reproductive disorders impose a major global burden. Infertility affects a large share of adults. Endometriosis is common in reproductive-age individuals and associates with pelvic pain and subfertility. Heavy menstrual bleeding drives anemia and reduces quality of life. Endometrial cancer ranks among the most common cancers in women worldwide.[8] These facts create a clear need for models that recapitulate epithelial structure and function with translational fidelity.

Existing *in vitro* systems leave gaps. Two-dimensional monolayers often lose polarity and hormone responsiveness. Organoids preserve epithelial architecture, yet they fall short on cycle-long barrier readouts and flow-dependent cues. Recent endometrium-on-a-chip studies have advanced the field: Busch *et al.*[9] built a patient-derived tri-culture uterine-wall model with functional readouts; Ahn *et al.*[10] engineered a vascularized endometrium-on-a-chip that captures epithelial–stromal–endothelial crosstalk; Gnecco *et al.*[11] showed that hemodynamic forces enhance decidualization *via* endothelial prostanoids; Kuperman *et al.*[12] exposed a tissue-engineered endometrial barrier to peristaltic-like shear and quantified the response. Most recently, a methods in molecular biology protocol detailed the formation of an organoid-derived endometrial epithelial monolayer on chip and a quantitative blastoid-adhesion assay, underscoring the uptake of the organoid-to-chip workflow.[13] Broader

[a] *KU-KIST Graduate School of Converging Science and Technology, Korea University, Seoul, Republic of Korea. E-mail: sidchung@korea.ac.kr*
[b] *School of Mechanical Engineering, Korea University, Seoul, Republic of Korea*
[c] *Center for Brain Technology, Brain Science Institute, Korea Institute of Science and Technology (KIST), Seoul, Republic of Korea*
[d] *Department of Obstetrics and Gynecology, Yonsei University College of Medicine, Seoul, Republic of Korea. E-mail: JUNGYUNLEE@yuhs.ac*
[e] *Biohybrid Systems Group, Coulter Department of Biomedical Engineering, Georgia Institute of Technology & Emory University School of Medicine, Atlanta, GA 30322, USA. E-mail: jihee.won@emory.edu*
[f] *Bupyeong Apple Obstetrics and Gynecology Clinic, Incheon, Republic of Korea*
[g] *Department of Obstetrics and Gynecology, Soonchunhyang University Bucheon Hospital, Bucheon, Republic of Korea*
[h] *Organoid Innovation Center, Biomedical Research Institute of Jeonbuk National University Hospital, Jeonju, Republic of Korea*
[i] *Einocle Inc, Seoul, Republic of Korea*
† Equal contribution as the first author.

reproductive-tract platforms extend scope: Xiao *et al.*[14] linked organ chips to reproduce a 28-day menstrual-cycle hormone profile, and Campo *et al.*[15] reviewed microphysiological endometrium models and routes to clinical relevance.

We address the remaining gap. Prior models validated triculture, vascularization, flow-dependent cues, and endocrine control; the field still lacks a device- and ECM-parameterized map for building a polarized epithelial monolayer from patient-derived organoids, with explicit barrier readouts under defined coatings/hydrogels and donor-to-donor variability reported as design constraints. Here, we build that map: a microfluidic epithelial model from patient-derived endometrial organoids with specified geometry, surface treatments, and ECM conditions. We quantify the epithelial morphology and barrier-related readouts and report donor variability as design constraints. This platform lays the foundation for adding stromal and immune components in a modular co-culture-on-chip.

Materials and methods

IRB information

The present study was reviewed and approved by our Institutional Review Board of Severance Hospital (4-2018-0928) in accordance with the Declaration of Helsinki and the International Conference on Harmonisation Good Clinical Practice guidelines.

Isolation of human endometrial epithelial cells and organoid culture

With informed consent, endometrial tissue was obtained from polyp resections in two donors (ages 27 (donor #1) and 37 (donor #2)). Detailed donor metadata are provided in Table S4. Epithelial cells were isolated by mechanical mincing with sterile scissors followed by enzymatic digestion in DMEM/F12 containing collagenase I (1 mg mL^{-1}; Worthington), dispase II (0.4 mg mL^{-1}; Sigma-Aldrich), penicillin (100 U mL^{-1}; Gibco), and streptomycin (100 μg mL^{-1}; Gibco). The epithelial fraction was maintained in organoid expansion medium (ExM; composition in Table S1). Cells were mixed with Matrigel (Corning) and seeded as domes on culture plates, and then cultured in ExM. Organoids were passaged every nine days. For all experiments, we used early-passage organoids (p5–p8).

Fabrication and preparation of microfluidic devices

Microfluidic devices comprising a one gel channel and two media channels were fabricated, as previously described.[16] Detailed device dimensions are provided in Fig. S1. The PDMS (SYLGARD 184; Dow Corning) base and curing agent were mixed at an 8 : 1 ratio, poured onto a patterned wafer, and cured at 80 °C. The cured PDMS was cut, sterilized, dried, and—after plasma treatment—irreversibly bonded to glass coverslips (Paul Marienfeld, Germany). For surface treatment, 60 μL of either polydopamine (PDA; dopamine hydrochloride 2 mg mL^{-1} in Tris-HCl, pH 8.5, Sigma-Aldrich) or poly-D-lysine (PDL; 1 mg mL^{-1} in DI (distilled, deionized) water, Sigma-Aldrich) solution was introduced to coat the channel walls. PDA-treated devices were incubated at room temperature for 2 h; PDL-treated devices were incubated at 37 °C for 1 h. The devices were then rinsed three times with DI water and dried at 80 °C overnight. Gel regions were filled with 10 μL of reconstituted rat-tail type I collagen (COL1; Corning) at 2, 3, 4, or 5 mg mL^{-1}, neutralized to pH 7.4 with 10× PBS and 0.5 N NaOH. Collagen was polymerized at 37 °C for 30 min. Media channels were then filled with culture medium, and devices were kept at 37 °C until use. For basement-membrane (BM) coating, Matrigel diluted to 2% (v/v) in DMEM/F12 was introduced into the cell-seeding channel and left for 30 min; all steps—from solution preparation to coating—were conducted under ice-cold conditions, followed by a brief cold rinse.

Culture of endometrial organoids in the microfluidic device

We harvested cells from organoids by removing Matrigel and dissociating the tissue. Organoids were collected, washed with ice-cold PBS, and centrifuged at 2000 rpm for 3 min at 4 °C. The supernatant and residual Matrigel above the pellet were carefully removed. The pellet was then dissociated to single cells with TrypLE (Gibco) at 37 °C for 7 min, followed by enzyme neutralization. The cells were collected by centrifugation (1000 rpm, 5 min), and resuspended to 1.5×10^6 cells per mL. For seeding, 60 μL of the cell suspension was introduced into a medium channel. The devices were oriented vertically to position cells along the collagen hydrogel wall and incubated at 37 °C for 2 h to allow attachment. Each channel was then filled with up to 120 μL of culture medium, and the devices were maintained at 37 °C, 5% CO_2. The culture medium was replaced daily.

Human uterine fibroblast culture and epithelial–fibroblast co-culture

Fibroblast culture. Primary human uterine fibroblasts (HUF; ATCC PCS-460-010) were expanded in Fibroblast Basal Medium (ATCC PCS-201-030) supplemented with one Fibroblast Growth Kit—Low Serum (ATCC PCS-201-041), following the manufacturer's instructions. Cells were maintained at 37 °C, 5% CO_2, and passaged at ~70–80% confluence using TrypLE. Viable cells were counted by trypan blue exclusion before embedding.

Fluorescent labeling. Organoid-derived epithelial cells were stably labeled with mCherry and human uterine fibroblasts with GFP by lentiviral transduction. Transduced cells were selected with puromycin (0.5 μg mL^{-1}, over 2 passages) and expanded. Labeled cells showed no detectable change in the morphology or growth.

Fibroblast embedding in COL1. On ice, fibroblasts were resuspended at 6×10^6 cells per mL in type I collagen (COL1) 5 mg mL^{-1} neutralized to pH 7.4, as described above. 10 μL of the cell–collagen suspension was introduced into the gel channel and polymerized at 37 °C for 30 min. Media

channels were filled with culture medium and equilibrated at 37 °C.

Epithelial seeding for co-culture. We seeded epithelial cells for co-culture as described above.

Hormone treatment of endometrial organoids and microfluidic devices

Organoids were cultured in ExM for 4 days after passaging, and then subjected to hormonal stimulation. For microfluidic devices, the cells were maintained in ExM for the first 48 h after seeding and then treated. Hormone exposure lasted 6 days under the following regimens: untreated (ExM only); E2: ExM for 2 days followed by 10 nM β-estradiol for 4 days; E2+P4+cAMP: ExM for 2 days and 10 nM β-estradiol for 2 days followed by 10 nM β-estradiol + 1 μM progesterone + 1 μM 8-bromoadenosine 3′,5′-cyclic monophosphate (8-Br-cAMP) for 2 days. Culture medium (and hormones for treated groups) was replaced daily. Reagent details are listed in Table S1.

Immunofluorescence staining

Organoids. Organoids were washed 3× with ice-cold PBS to remove residual Matrigel, fixed overnight at 4 °C in 4% paraformaldehyde (PFA in PBS; Biosesang), and rinsed with PBS. Samples were cryoprotected sequentially in 15% sucrose (overnight, 4 °C) and 30% sucrose (overnight, 4 °C), embedded in OCT, and cryosectioned at 9 μm. Sections were air-dried, OCT was removed with PBS + 0.05% Tween-20 (wash buffer), permeabilized with 0.1% Triton X-100 in PBS, and blocked in 3% BSA in PBS (Thermo Scientific). After blocking, the sections were washed with PBS and incubated overnight at 4 °C with primary antibodies diluted in 3% BSA/PBS. Following washes, the sections were incubated for 2 h at room temperature (RT, protected from light) with Alexa Fluor 488-conjugated secondary antibodies (1 : 500; Invitrogen), DAPI (1 : 1000; Invitrogen), and rhodamine-phalloidin (1 : 400; Invitrogen), washed with PBS, and mounted (Vector Laboratories).

Microfluidic devices. Media were removed and devices were washed with wash buffer. Cells were fixed with 4% PFA for 30 min at RT on a rocker, and then washed with wash buffer. Permeabilization was performed with 0.5% Triton X-100 in PBS for 30 min at RT, followed by washing and blocking with 3% BSA/PBS for 2 h at RT. Primary antibodies diluted in 3% BSA/PBS were introduced and incubated for 2 days at 4 °C on a rocker. After washing, Alexa Fluor 488-conjugated secondary antibodies (1 : 500; Invitrogen), DAPI (1 : 1000; Invitrogen), and rhodamine-phalloidin (1 : 400; Invitrogen) in 3% BSA/PBS were applied for 2 days at 4 °C with gentle rocking (protected from light). The devices were then washed repeatedly with wash buffer for 2 days at 4 °C and stored in PBS at 4 °C until imaging. The primary antibodies are listed in Table S2.

Gene expression analysis by qRT-PCR

Total RNA from organoids and microfluidic device cultures was isolated using TRIzol (Thermo Fisher Scientific) and quantified with a NanoDrop spectrophotometer. cDNA was synthesized with a High-Capacity RNA-to-cDNA kit (Invitrogen) following the manufacturer's instructions. qRT-PCR was performed with a QuantiTect SYBR Green PCR Kit (Qiagen). Relative gene expression was calculated by the ΔΔCt method using GAPDH as the reference gene. Primer sequences are listed in Table S3.

Hematoxylin and eosin (H&E) staining and immunohistochemistry (IHC)

Formalin-fixed (4% PFA) endometrial tissue was dehydrated through graded ethanol (50%, 70%, 80%, 90%, 95%, and 100%), cleared in xylene (Sigma-Aldrich), and embedded in paraffin. Paraffin blocks were sectioned, and the sections were deparaffinized in xylene and rehydrated through graded ethanol to water. For H&E, sections were stained sequentially with hematoxylin and eosin, dehydrated, cleared, and mounted. For IHC, antigen retrieval was performed by heat-induced epitope retrieval (HIER). Sections were blocked in 2% serum (matched to the secondary antibody host) in PBS

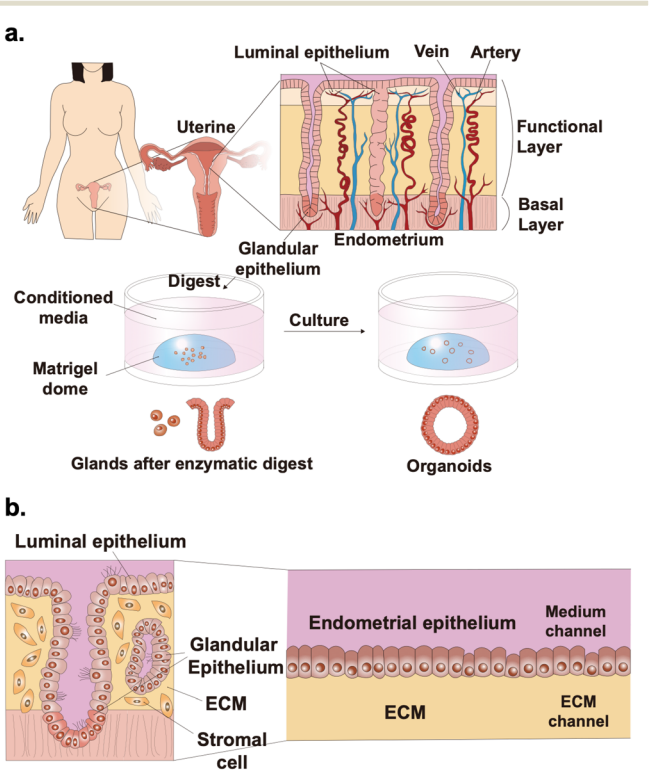

Fig. 1 Workflow and model architecture. a. Derivation of patient-derived endometrial organoids from the glandular epithelium isolated from clinical specimens and expanded in Matrigel domes. b. Schematic of the microfluidic model showing a polarized endometrial epithelial layer along the epithelial (endometrium) channel adjacent to an ECM (gel) channel; inset depicts the corresponding *in vivo* glandular epithelium–stroma interface.

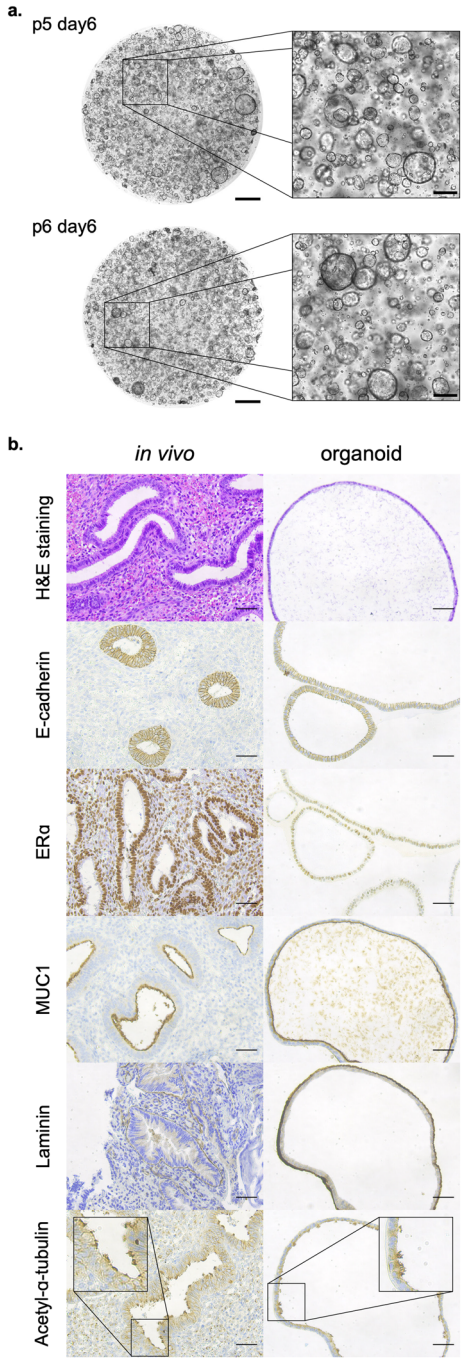

Fig. 2 Morphology and marker expression in patient-derived endometrial organoids *versus* human endometrium. a. Bright-field images of endometrial organoids showing the typical cystic architecture (examples from p5 and p6, day 6). Scale bars: left, 1 mm; magnified insets, 250 μm. b. Histology and immunohistochemistry of human endometrium and matched organoids. H&E and IHC localize E-cadherin (epithelial junctions), ERα (nuclear estrogen receptor), MUC1 (apical surface), laminin (basement-membrane interface), and acetyl-α-tubulin (cilia). Marker distributions in organoids recapitulate those in tissue. Scale bars: 50 μm.

and incubated with primary antibodies for 30 min at room temperature. Biotinylated secondary antibodies were applied, followed by Vectastain ABC-HRP (Vector) and development with DAB (Sigma-Aldrich). The sections were counterstained with hematoxylin and mounted using a glycerol/gelatin mounting medium (Sigma-Aldrich). The primary antibodies are listed in Table S2.

Quantification of epithelial confluency and hydrogel degradation

In Fig. 6c, epithelial cell attachment is quantified from phase-contrast images in the reservoir channel. A rectangular region of interest spanning the full channel width and a longitudinal length corresponding to four post intervals was selected per device, and the number of epithelial nuclei within this region was counted and reported as the number of cells per region of interest. In Fig. 6d, hydrogel degradation is quantified relative to the initial gel–medium interface at day 0, defined at the narrow post gap bordering the reservoir channel. At each time point, the region of collagen that had been eroded or invaded by cells beyond this interface is manually outlined and its area measured.

Barrier permeability assay and Fick's law analysis

Signal detection. To quantify macromolecular transport across the epithelial–hydrogel interface, we performed a 70 kDa FITC–dextran permeability assay in devices with and without an epithelial monolayer. After equilibration in culture medium, 70 kDa FITC–dextran was introduced into the epithelial (luminal) channel, while the opposite channel contained a tracer-free medium. Time-lapse fluorescence images (GFP channel) were acquired at 37 °C every 10 min for 180 min using identical exposure settings for all conditions. For each frame, fluorescence intensity was averaged over the channel height and expressed as a function of distance (x) orthogonal to the

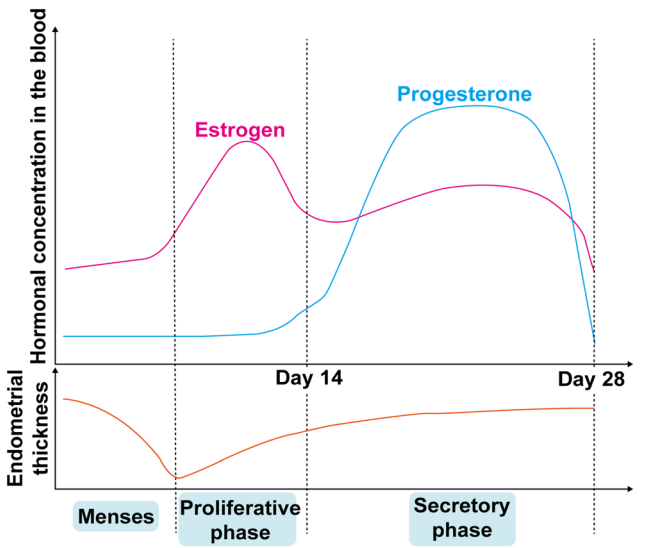

Fig. 3 Representative profiles of circulating estradiol and progesterone across the menstrual cycle, with the corresponding change in the endometrial thickness (menses, proliferative, and secretory phases).

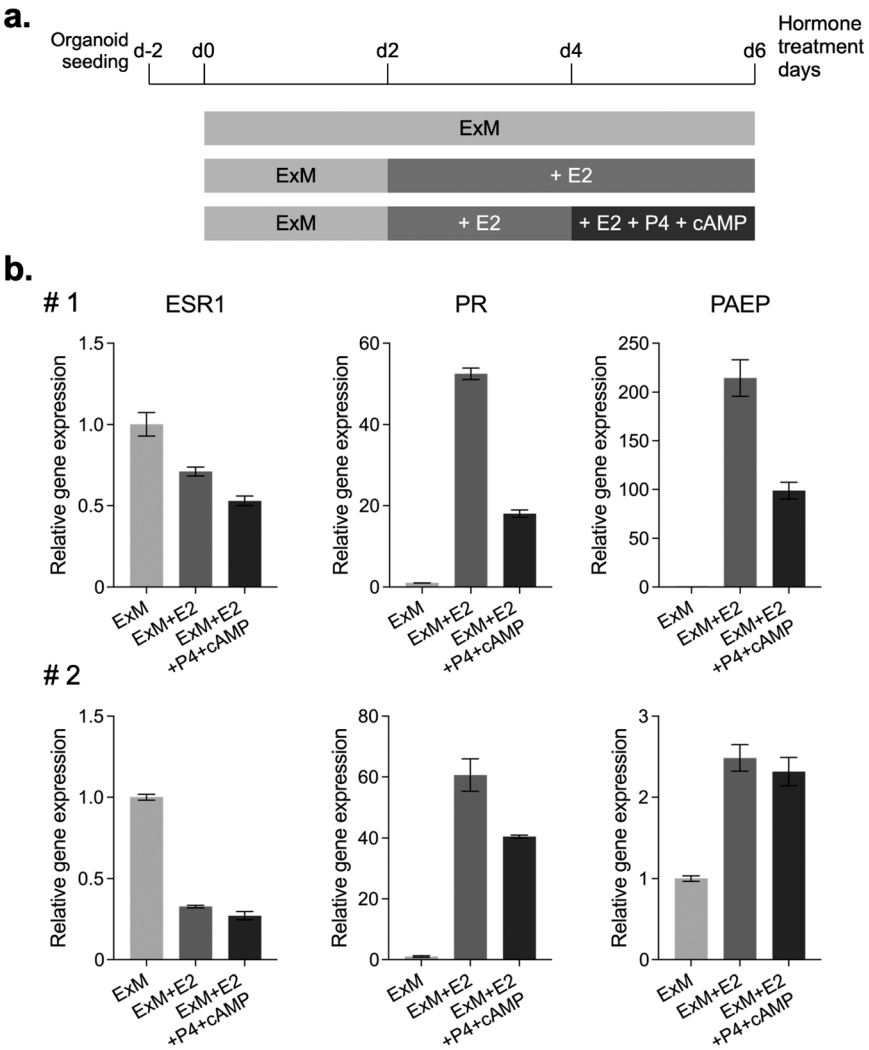

Fig. 4 Hormone-responsive gene expression in patient-derived endometrial organoids. a. Experimental schedule for hormone stimulation in endometrial organoids and microfluidic devices. b. qRT-PCR of ESR1, PR, and PAEP in organoids from donors #1 and #2 under the indicated conditions.

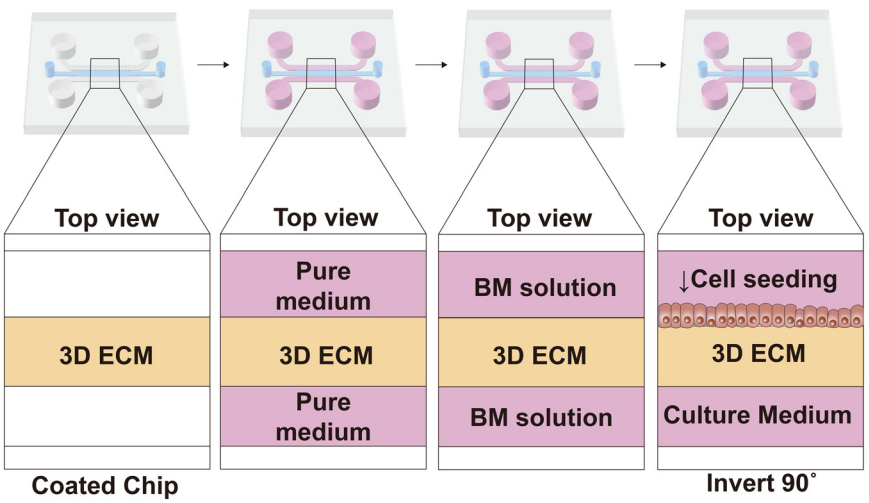

Fig. 5 Seeding workflow in the microfluidic device (top-view schematics).

epithelial–hydrogel interface. Intensities were normalized to the mean intensity in the epithelial channel region ($x \approx -140$ μm), and the resulting normalized profiles were used as a proxy for relative dextran concentration.

Fick's first law. Under the assumption of one-dimensional diffusion across the hydrogel and negligible depletion of tracers in the source channel, a permeability (P) was computed from Fick's first law as the proportionality between diffusive flux at

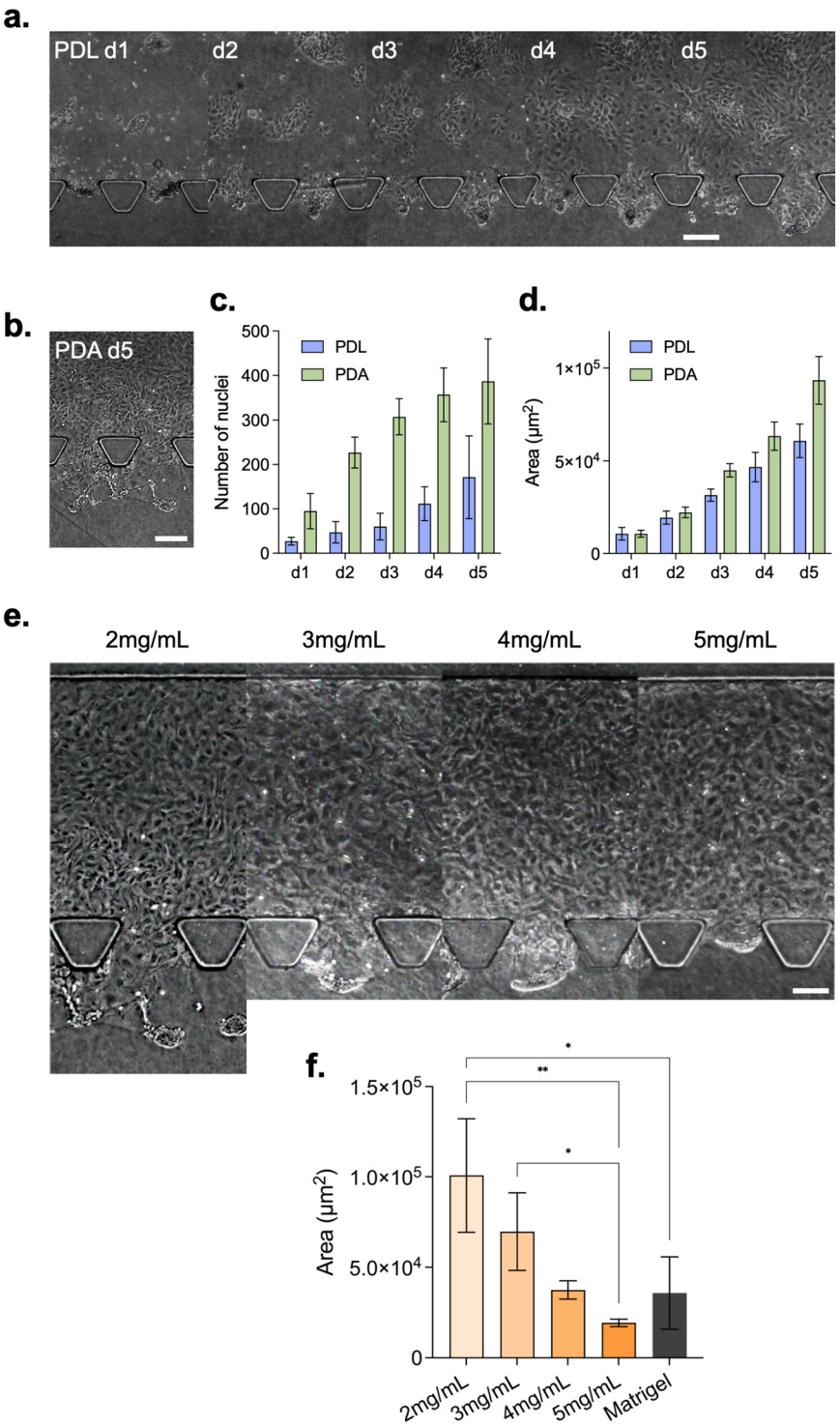

Fig. 6 Surface treatment and collagen stiffness govern epithelial layer stability on-chip. a. Time course (d1–d5) on PDL-coated devices showing poor retention and hydrogel erosion. b. PDA-coated device (d5) with improved epithelial coverage. c. Quantification of cells adhering to the channel surface (d1–d5) on PDL- *vs.* PDA-coated devices (nuclei counts). d. Quantification of the degraded hydrogel area (d1–d5) on PDL- *vs.* PDA-coated devices. e. Collagen I gels 2–5 mg mL^{-1}: higher concentrations reduce hydrogel degradation. f. Quantification of the degraded area across collagen concentrations and Matrigel. Scale bar: 200 μm.

the epithelial–hydrogel interface and the concentration difference between the epithelial channel and the hydrogel. The diffusion coefficient (D) of 70 kDa dextran was set to 7.0×10^{-7} $cm^2\ s^{-1}$, consistent with reported values in aqueous media, and treated as a constant for all conditions. The concentration gradient dC/dx was estimated by the linear fitting of the normalized fluorescence profile in the 0–350 μm hydrogel region at each time point, and the diffusive flux was calculated as $J = -D \cdot dC/dx$. The permeability was then obtained from $P = -J/\Delta C$, where ΔC is the concentration difference between the epithelial channel and the hydrogel. Because D and the intensity–concentration proportionality factor act as common prefactors, changes in P between gel-only and epithelial devices primarily report changes in the barrier function.

Results and discussion

Establishing patient-derived endometrial organoids

We generated endometrial organoids from cells isolated from human endometrial polyp specimens (Fig. 1a).[17] As shown in the schematic, we compartmentalized the microfluidic device into an ECM channel and a cell-seeding channel to model the *in vivo* interface (Fig. 1b). We optimized ECM stability by loading type I collagen (COL1) into the hydrogel channel and adding a thin Matrigel coating, and then seeded dissociated endometrial epithelial cells onto this ECM barrier to form a continuous endometrial epithelial layer (Fig. 5a). These human tissue-derived organoids showed the expected cystic architecture, and this morphology persisted across passages (p5–p6; Fig. 2a). We benchmarked the organoids against the *in vivo* endometrium by immunohistochemistry (Fig. 2b). E-Cadherin marked epithelial junctions, and ERα was expressed in a pattern consistent with *in vivo* tissue. We assessed apicobasal polarity with MUC1 (apical gland marker) and laminin (basement-membrane/ECM marker). Because MUC1 varies across the uterine cycle,[18] the organoid MUC1 pattern indicates a proliferative-phase state. Laminin deposition appeared along the basal surface at the epithelial–ECM interface. Acetyl-α-tubulin, a cilia marker, was also present in the organoids. Together, these data show reproducible organoid generation with *in vivo*-like histology, consistent with prior reports by Boretto *et al.* and Turco *et al.*[17,19]

The endometrium remodels across the proliferative, secretory, and menstrual phases in step with changing circulating sex steroids. Unlike other mucosal epithelia, it shows marked responsiveness to ovarian hormones—estrogen and

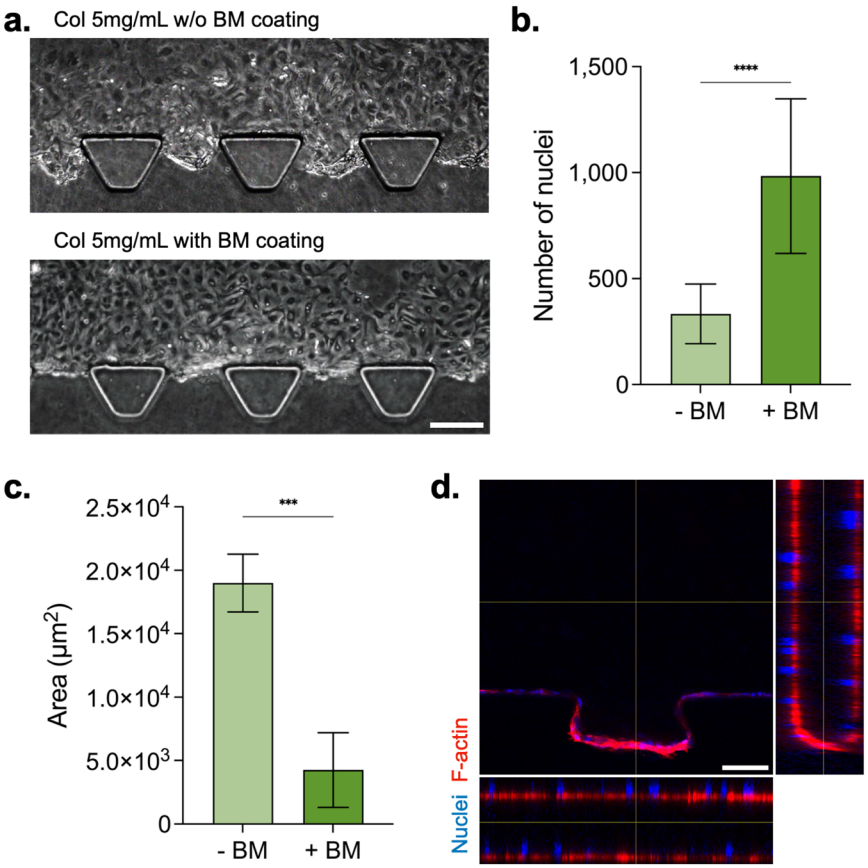

Fig. 7 Basement-membrane (BM) coating improves adhesion and limits hydrogel degradation. a. Phase-contrast images of COL1 5 mg mL^{-1} devices without (top) and with (bottom) BM coating. Scale bar: 200 μm. b. Cells adhering to the channel surface (nuclei counts) with and without BM coating on PDA-treated devices. c. Degraded hydrogel area is reduced by BM coating. d. Confocal orthogonal view showing a continuous epithelial monolayer along the hydrogel interface (DAPI, blue; F-actin, red). Scale bar: 100 μm.

progesterone—that drive the uterine cycle (Fig. 3).[1] To evaluate the organoids' ability to replicate physiological characteristics of the endometrial epithelium, we quantified the hormone-responsive mRNA expression of ESR1 (estrogen receptor α), PR (progesterone receptor), and PAEP (progestogen-associated endometrial protein) by qRT-PCR after the hormone treatments, as shown in Fig. 4a.[17] ESR1 and PR are intranuclear receptors in endometrial cells that respond to estrogen and progesterone, respectively. Their mRNA levels vary across the menstrual cycle, increasing during the proliferative phase and decreasing during the secretory phase,[20,21] and recent *in vitro* organoid studies reported similar patterns.[17] PAEP increases in a stage-specific manner because of its role in pregnancy-related cellular immune activity.[22] In our organoids, we observed decreased ESR1 under the proliferative-phase conditions (+E2) and decreased PAEP under the secretory-phase conditions (+E2+P4+cAMP), in contrast to their broader expression *in vivo* (Fig. 4b).

Building a 3D endometrial epithelium on a microfluidic chip

Using the procedure shown in Fig. 5, we established a 3D microchannel model and formed an endometrial epithelial layer along the interface with the ECM hydrogel scaffold. We PDL-coated the device, filled the ECM channel with type I collagen (COL1, 2 mg mL^{-1}) to gel, and then loaded single cells dissociated from endometrial organoids. We aimed to form a continuous monolayer across the hydrogel region. However, the collagen scaffold progressively degraded and collapsed, which impeded stable monolayer formation (Fig. 6a). We varied the surface coatings and ECM conditions. Polydopamine (PDA), formed by oxidative self-polymerization of dopamine hydrochloride in Tris-HCl buffer, creates an adhesive interlayer for the surface and cells.[23] Compared with PDL, PDA-coated devices showed progressively higher epithelial coverage of the reservoir channel over 5 days, and the difference in nuclei counts between coatings widened with time (Fig. 6b and c). By day 5, the number of epithelial nuclei on PDA reached 386.75 ± 95.34 cells per region of interest, representing an approximately 2.3-fold increase over PDL (171.25 ± 93.30) cells per region (Fig. 6c). Despite this increased cell attachment, the collagen hydrogel was still progressively invaded and degraded on both coatings. The degraded area increased over 5 days with an expanding separation between the PDL and PDA conditions (Fig. 6d). By day 5, the degraded area reached 6.1 ± 0.9 × 10^4 μm^2 per

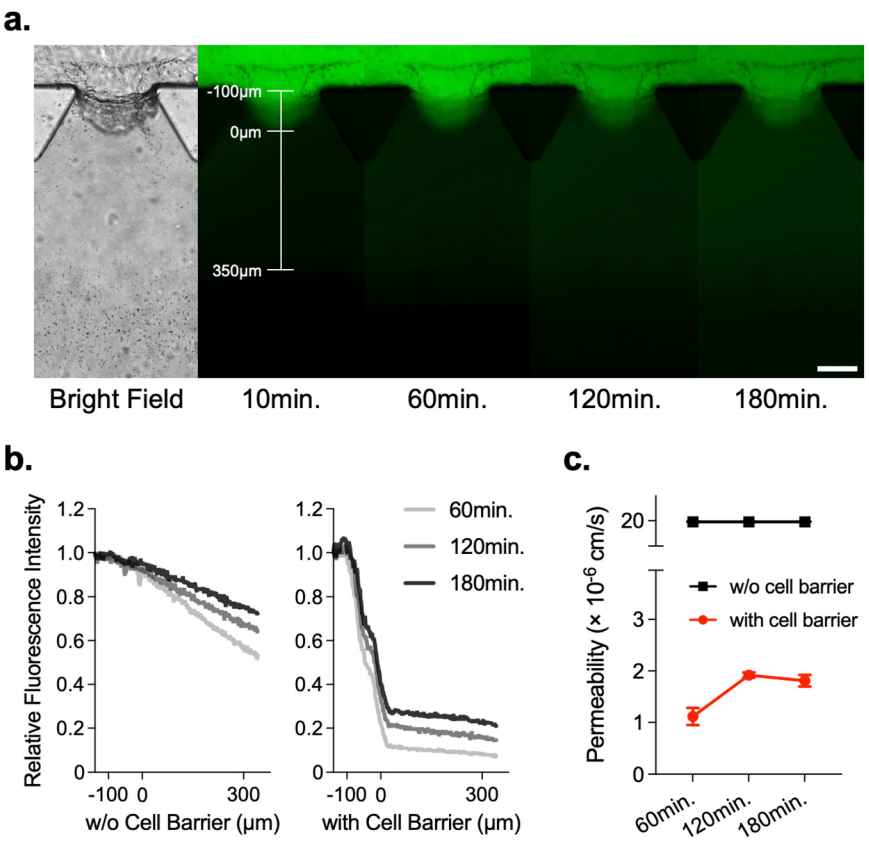

Fig. 8 Barrier permeability of the on-chip endometrial epithelium. a. Time-lapse fluorescence showing diffusion from the epithelial channel across the hydrogel; the fluorescence gradient is maintained up to 180 min. Scale bar: 100 μm. b. Spatial fluorescence profiles without (left) and with (right) a cell barrier at 60, 120, and 180 min; the on-chip monolayer produces a sharp drop and reduced penetration. Barrier position: 0 μm. c. Permeability (cm s^{-1}) computed from Fick's first law for conditions without and with a cell barrier; without a cell barrier, permeability remains high and constant over time, whereas with a barrier, values plateau after ~120 min, indicating a stable, time-invariant barrier.

region in PDL devices and 9.3 ± 1.3 × 10^4 μm^2 per region in PDA devices, corresponding to an approximately 1.5-fold difference between coatings (Fig. 6d), indicating that collagen erosion remained a major failure mode that ultimately prevented the formation of a stable monolayer. We increased the COL1 concentration to stiffen the hydrogel and prevent scaffold collapse in the PDA-coated condition. Prior studies show that type I collagen gels exhibit concentration-dependent increases in modulus and network density.[24–27] In our chips, the area of cell-induced hydrogel degradation decreased monotonically from 2 to 5 mg mL^{-1}. By day 5, the degraded area at COL1 5 mg mL^{-1} was reduced to ~19% of that at 2 mg mL^{-1} (≈5.2-fold reduction), and COL1 5 mg mL^{-1} showed less loss of the scaffold than Matrigel in the same geometry (Fig. 6e and f). Given that the endometrial stromal ECM is rich in fibrillar collagens (notably type I), whereas Matrigel is a basement-membrane extract (laminin/collagen IV-dominant) with batch variability, a COL1-based scaffold better represents the stromal compartment for epithelial–stromal interface studies.[28–30] We next built on the most stable conditions (COL1 5 mg mL^{-1}) by adding a basement-membrane-mimicking the Matrigel coating. This PDA-to-BM coating increased cell attachment on the channel surface and yielded uniform confluency (Fig. 7a and b). By day 5, the number of epithelial nuclei with BM coating was approximately 3.0-fold higher than with PDA alone, whereas the degraded hydrogel area was reduced to ~22% of the PDA conditions (~4.5-fold reduction; Fig. 7c). Confocal imaging confirmed a continuous, polarized epithelial monolayer spanning the hydrogel interface (Fig. 7d).

The on-chip epithelium forms a stable, structurally intact monolayer

We next evaluated the barrier function using a 70 kDa FITC–dextran permeability assay in devices with and without an epithelial monolayer and quantified a permeability from Fick's first law as described in the methods (Fig. 8). In gel-only devices, dextran rapidly penetrated the hydrogel, the fluorescence profiles across the gel became nearly flat over time, and the permeability remained high and essentially constant throughout the 180 min measurement (Fig. 8b, c and S2). In contrast, when a confluent epithelial monolayer lined the channel, the fluorescence profiles preserved a sharp concentration step at the epithelial–hydrogel interface, intensities in the hydrogel region remained low, and the permeability reached a plateau after ~120 min that was unchanged at 180 min (Fig. 8b and c). At 180 min, the permeability with a cell barrier was 1.81 ± 0.11 × 10^{-6} cm s^{-1}, which was approximately 11-fold lower than in gel-only devices (19.96 ± 0.005) × 10^{-6} cm s^{-1}; n = 3 devices. These data indicate an intact epithelial barrier that limits macromolecular transport across the hydrogel interface. The plateau in permeability after 120 min indicates a quasi–steady-state diffusion regime consistent with Fick's first law in chip-based barrier assays, and the marked reduction *versus* gel-only controls is in line with best-practice barrier measurements in organ-on-chip systems.[31,32] The endometrial epithelium forms tight junctions, providing a structural basis for the size-selective restriction of macromolecules such as 70 kDa dextran.[33] We assessed epithelial identity and polarity by immunofluorescence (Fig. 9). The ERα localized to nuclei, consistent with an estrogen-responsive endometrial epithelium. Acetyl-α-tubulin marked apical cilia, indicating ciliogenesis at the luminal surface. Laminin outlined the basal interface at the epithelium–ECM boundary, defining a basement-membrane-like a layer along the

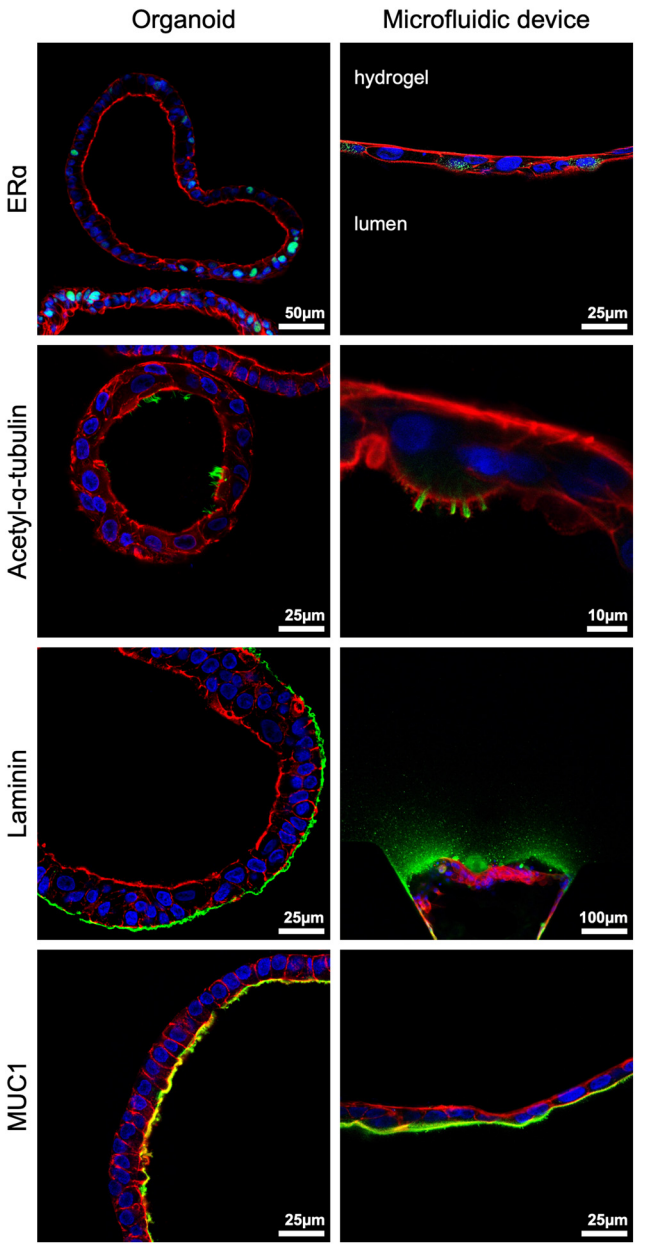

Fig. 9 Polarized marker localization in organoids and on-chip epithelium. Immunofluorescence of ERα (nuclear receptor), acetyl-α-tubulin (apical cilia), laminin (basal basement-membrane interface), and MUC1 (apical membrane) comparing organoids (left) and the microfluidic epithelium (right). Green: target markers; blue: nuclei; red: F-actin.

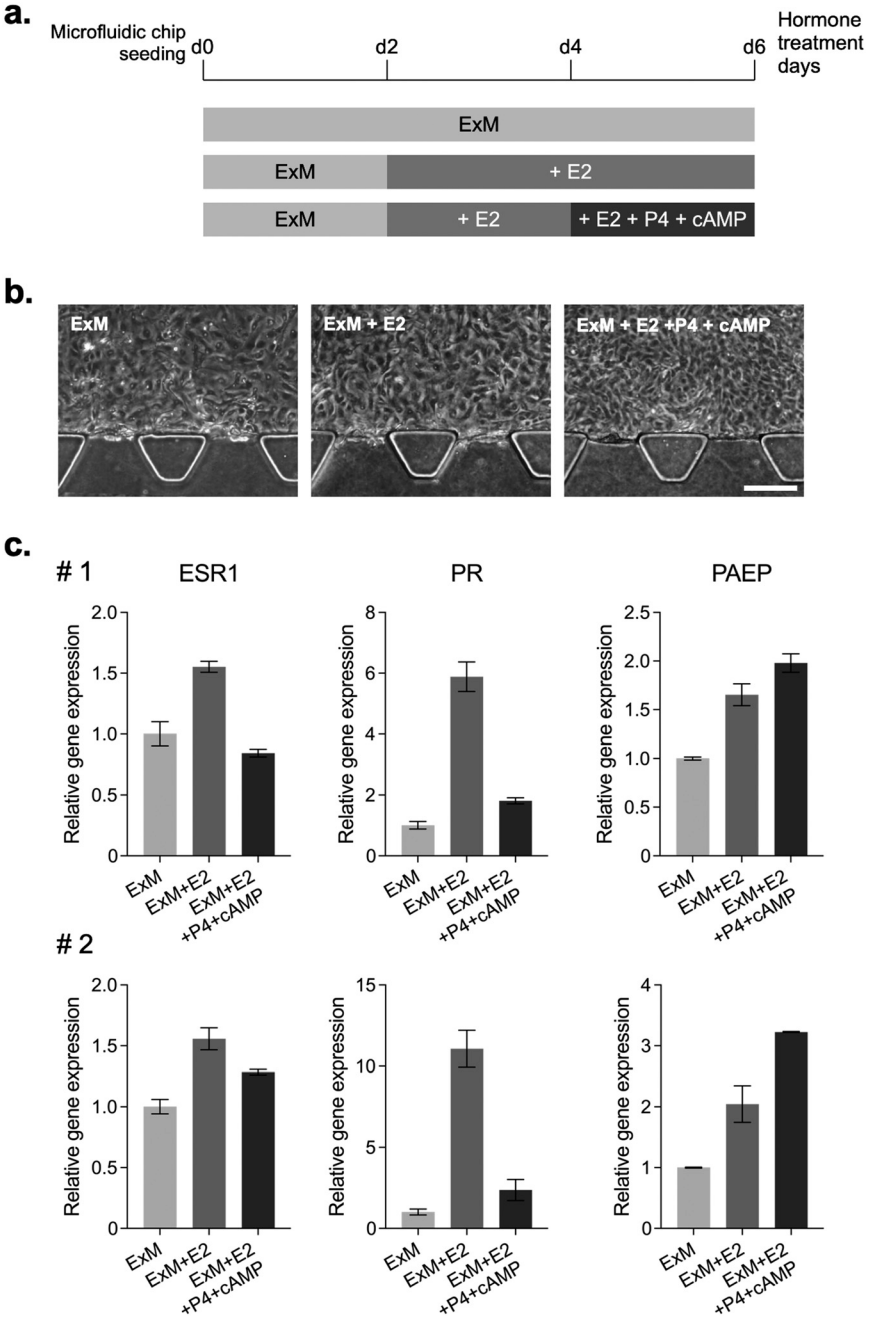

Fig. 10 Hormone responsiveness of the collagen-based on-chip endometrial epithelium. a. Hormone regimen applied after seeding. b. Phase-contrast images showing an increased epithelial density under E2 and E2+P4+cAMP compared with ExM. Scale bar: 200 μm. c. qRT-PCR of ESR1, PR, and PAEP for donors #1 and #2 under the indicated conditions.

hydrogel side. MUC1, an apical membrane glycoprotein, concentrated at the luminal border. These spatial patterns—nuclear ERα, apical acetyl-α-tubulin and MUC1, and basal laminin—demonstrate a polarized, differentiated monolayer on chip and mirror the distribution observed in the paired organoids. We applied the organoid hormone regimen to the on-chip epithelium (Fig. 10a). Under E2, the epithelial sheet became denser than in ExM alone and remained dense under the E2+P4+cAMP condition (Fig. 10b), indicating E2-driven proliferation with subsequent maturation. We then quantified ESR1, PR, and PAEP by qRT-PCR. ESR1 and PR increased with E2 and decreased after E2+P4+cAMP, whereas PAEP rose from the proliferative-to-secretory-phase condition (Fig. 10c). Both donors showed the same directional trends. Notably, the same transcriptomic pattern observed in organoids emerged on chip under the matched regimen, supporting reproducibility across donors and transferability of the protocol across culture platforms. As a comparison, a Matrigel-scaffold device showed a blunted transcriptional response to the same sequence despite comparable morphology (Fig. S3). Together, these data support

the COL1 scaffold plus PDA-BM coating as suitable conditions for building a functional, hormone-responsive endometrial epithelial layer on chip.

We built a 3D endometrial epithelium-on-chip from patient-derived organoids and treated this study as a pilot, parameter-optimization effort. We systematically linked device and ECM parameters to epithelial readouts—morphology and confluency, polarity markers (ERα, MUC1, acetyl-α-tubulin, and laminin), barrier function (70 kDa dextran permeability), and hormone-responsive transcripts (ESR1, PR, and PAEP)—and tracked donor-to-donor trends. This mapping identified COL1 5 mg mL^{-1} combined with PDA-to-BM coating as a stable condition that supports a polarized monolayer with low, time-invariant permeability and reproducible hormone responses across donors and across culture platforms (organoids and chip). The architecture also enables modular co-culture. When we embedded fibroblasts in COL1 (5 mg mL^{-1}) and applied the same BM coating + epithelial seeding workflow, stromal and epithelial compartments coexisted without interference in the device (Fig. S4). This demonstrates compatibility for stromal addition and sets the stage for immune and endothelial components. Together, these results establish a design space for building an endometrial epithelial barrier on chip and show that tissue-derived organoids are a reliable cell source for microphysiological modeling. The platform now supports targeted expansion—adding stromal, immune, and vascular cells—to interrogate multicellular crosstalk under controlled ECM and surface conditions.

Conclusion

We establish an organoid-to-chip workflow that yields a polarized, hormone-responsive endometrial epithelium. A single reproducible condition—COL1 5 mg mL^{-1} with PDA-to-BM coating—supports a low-permeability barrier and conserved ESR1/PR/PAEP responses across donors. The platform is modular for stromal, immune, and endothelial additions. Limitations include two donors; next steps are donor expansion and analysis of microenvironment composition according to donor sample characteristics.

Author contributions

Conceptualization: Seok Chung; methodology: Seung-cheol Shin, Yale Hahm and Seok Chung; investigation: Seung-cheol Shin, Yale Hahm and Yeju Jeong; resources: Yup Kim, Junsik Park and Jung-Yun Lee; formal analysis: Ji Hun Yang, Jin-A Kim and Jihee Won; validation: Ji Hun Yang, Jin-A Kim and Jihee Won; data curation: Seung-cheol Shin and Yale Hahm; writing – original draft: Seung-cheol Shin and Yale Hahm; writing – review & editing: Jihee Won and Seok Chung; supervision: Jihee Won, Jung-Yun Lee and Seok Chung. All authors discussed the results and approved the final version of the manuscript.

Conflicts of interest

There are no conflicts of interest to declare.

Data availability

This study was conducted using patient-derived cells approved by the IRB, and the relevant information is described in Materials and Methods. However, if additional data are needed to protect patient privacy, reasonable requests should be made to the corresponding author. Supplementary information (SI): the SI includes additional figures (Fig. S1–S4) and tables (Tables S1–S4), including medium composition/reagent details (Table S1), a primary antibody list (Table S2), qRT-PCR primer sequences (Table S3), and donor metadata (Table S4). See DOI: https://doi.org/10.1039/d5lc00278h.

Acknowledgements

This research was supported by a grant of the Korea Health Technology R&D Project through the Korea Health Industry Development Institute (KHIDI), funded by the Ministry of Health & Welfare, Republic of Korea (grant number: HI19C0263), and S.-C. Shin, Y. Jeong, J.-A Kim & S. Chung were supported by MOTIE Technology Innovation Program (TIP) (RS-2025-02310813) and the MOTIE Alchemist Project (2410012609; 20012378).

References

1 L. Deligdisch, *Mod. Pathol.*, 2000, **13**, 285–294.
2 T. Maruyama and Y. Yoshimura, *Endocr. J.*, 2008, **55**, 795–810.
3 A. Pedram, M. Razandi, M. Lewis, S. Hammes and E. R. Levin, *Dev. Cell*, 2014, **29**, 482–490.
4 A. Roy and M. M. Matzuk, *Nat. Rev. Endocrinol.*, 2011, **7**, 517–525.
5 H. J. Mertens, M. J. Heineman, P. H. Theunissen, F. H. de Jong and J. L. Evers, *Eur. J. Obstet. Gynecol. Reprod. Biol.*, 2001, **98**, 58–65.
6 M. SEPPÄLÄ, M. JULKUNEN, A. KOSKIMIES, T. LAATIKAINEN, U. H. STENMAN and M.-L. HUHTALA, *Ann. N. Y. Acad. Sci.*, 1988, **541**, 432–444.
7 D. M. Berman, *Int. J. Gynecol. Pathol.*, 2002, **21**, 426.
8 F. Bray, M. Laversanne, H. Sung, J. Ferlay, R. L. Siegel, I. Soerjomataram and A. Jemal, *Ca-Cancer J. Clin.*, 2024, **74**(3), 229–263.
9 C. Busch, C. J. Hill, K. Paterson, R. Mellin, M. Zagnoni, D. K. Hapangama and M. E. Sandison, *Hum. Reprod.*, 2024, **39**(11), 2537–2550.
10 J. Ahn, M. J. Yoon, S. H. Hong, H. Cha, D. Lee, H. S. Koo and Y. J. Kang, *Hum. Reprod.*, 2021, **36**(10), 2720–2731.
11 J. S. Gnecco, T. Ding, C. Smith, J. Lu, K. L. Bruner-Tran and K. G. Osteen, *Hum. Reprod.*, 2019, **34**(4), 702–714.
12 D. Elad, U. Zaretsky, T. Kuperman, M. Gavriel, M. Long, A. Jaffa and D. Grisaru, *APL Bioeng.*, 2020, **4**(2), 026107.

13 A. Ak, D. Luijkx, D. Carvalho, S. Giselbrecht, R. van Golde and E. Vrij, *Methods Mol. Biol.*, 2025, 1–17.
14 S. Xiao, J. R. Coppeta, H. B. Rogers, B. C. Isenberg, J. Zhu, S. A. Olalekan and T. K. Woodruff, *Nat. Commun.*, 2017, **8**(1), 14584.
15 H. Campo, A. Murphy, S. Yildiz, T. Woodruff, I. Cervello and J. J. Kim, *Tissue Eng., Part A*, 2020, **26**(13–14), 759–768.
16 Y. Shin, S. Han, J. S. Jeon, K. Yamamoto, I. K. Zervantonakis, R. Sudo, R. D. Kamm and S. Chung, *Nat. Protoc.*, 2012, **7**, 1247–1259.
17 M. Y. Turco, L. Gardner, J. Hughes, T. Cindrova-Davies, M. J. Gomez, L. Farrell, M. Hollinshead, S. G. E. Marsh, J. J. Brosens, H. O. Critchley, B. D. Simons, M. Hemberger, B. K. Koo, A. Moffett and G. J. Burton, *Nat. Cell Biol.*, 2017, **19**, 568–577.
18 U. Jeschke, H. Walzel, I. Mylonas, P. Papadopoulos, N. Shabani, C. Kuhn, S. Schulze, K. Friese, U. Karsten, D. Anz and M. S. Kupka, *J. Histochem. Cytochem.*, 2009, **57**, 871–881.
19 M. Boretto, B. Cox, M. Noben, N. Hendriks, A. Fassbender, H. Roose, F. Amant, D. Timmerman, C. Tomassetti, A. Vanhie, C. Meuleman, M. Ferrante and H. Vankelecom, *Development*, 2017, **144**, 1775–1786.
20 S. Matsuzaki, T. Fukaya, T. Suzuki, T. Murakami, H. Sasano and A. Yajima, *Mol. Hum. Reprod.*, 1999, **5**, 559–564.
21 S. Ingamells, I. G. Campbell, F. W. Anthony and E. J. Thomas, *J. Reprod. Fertil.*, 1996, **106**, 33–38.
22 A. Zieba, E. Sjostedt, M. Olovsson, L. Fagerberg, B. M. Hallstrom, L. Oskarsson, K. Edlund, A. Tolf, M. Uhlen and F. Ponten, *OMICS*, 2015, **19**, 659–668.
23 S. H. Ku, J. S. Lee and C. B. Park, *Langmuir*, 2010, **26**, 15104–15108.
24 B. A. Roeder, K. Kokini, J. E. Sturgis, J. P. Robinson and S. L. Voytik-Harbin, *J. Biomech. Eng.*, 2002, **124**, 214–222.
25 E. E. Antoine, P. P. Vlachos and M. N. Rylander, *Tissue Eng., Part B*, 2014, **20**(6), 683–696.
26 Y. L. Yang, L. M. Leone and L. J. Kaufman, *Biophys. J.*, 2009, **97**(7), 2051–2060.
27 C. B. Raub, A. J. Putnam, B. J. Tromberg and S. C. George, *Acta Biomater.*, 2010, **6**(12), 4657–4665.
28 S. G. Zambuto, I. Jain, K. B. Clancy, G. H. Underhill and B. A. Harley, *ACS Biomater. Sci. Eng.*, 2022, **8**(9), 3819–3830.
29 A. Passaniti, H. K. Kleinman and G. R. Martin, *J. Cell Commun. Signaling*, 2022, **16**(4), 621–626.
30 G. Benton, I. Arnaoutova, J. George, H. K. Kleinman and J. Koblinski, *Adv. Drug Delivery Rev.*, 2014, **79**, 3–18.
31 C. Soragni, T. Vergroesen, N. Hettema, G. Rabussier, H. L. Lanz, S. J. Trietsch and C. P. Ng, *STAR Protoc.*, 2023, **4**(1), 102051.
32 Y. B. Arık, M. W. Van Der Helm, M. Odijk, L. I. Segerink, R. Passier, A. Van Den Berg and A. D. Van Der Meer, *Biomicrofluidics*, 2018, **12**(4), 042218.
33 M. D. Orchard and C. R. Murphy, *Acta Histochem.*, 2002, **104**(2), 149–155.